Oncogenic KRAS engages an RSK1/NF1 pathway to inhibit wild-type RAS signaling in pancreatic cancer

Derek K. Cheng[a,b,c,1], Tobiloba E. Oni[a,b,d,1], Jennifer S. Thalappillil[a,b,e], Youngkyu Park[a,b], Hsiu-Chi Ting[a,b], Brinda Alagesan[a,b,c], Nadia V. Prasad[a,b], Kenneth Addison[a,b], Keith D. Rivera[a], Darryl J. Pappin[a], Linda Van Aelst[a], and David A. Tuveson[a,b,2]

[a]Cold Spring Harbor Laboratory, Cold Spring Harbor, NY 11724; [b]Lustgarten Foundation Pancreatic Cancer Research Laboratory, Cold Spring Harbor, NY 11724; [c]Graduate Program in Genetics, Stony Brook University, Stony Brook, NY 11794; [d]Graduate Program in Molecular and Cellular Biology, Stony Brook University, Stony Brook, NY 11794; and [e]Graduate Program in Molecular and Cellular Pharmacology, Stony Brook University, Stony Brook, NY 11794

Edited by Mariano Barbacid, Spanish National Cancer Research Centre, Madrid, Spain, and approved April 15, 2021 (received for review August 13, 2020)

Pancreatic ductal adenocarcinoma (PDAC) is a lethal malignancy with limited treatment options. Although activating mutations of the KRAS GTPase are the predominant dependency present in >90% of PDAC patients, targeting KRAS mutants directly has been challenging in PDAC. Similarly, strategies targeting known KRAS downstream effectors have had limited clinical success due to feedback mechanisms, alternate pathways, and dose-limiting toxicities in normal tissues. Therefore, identifying additional functionally relevant KRAS interactions in PDAC may allow for a better understanding of feedback mechanisms and unveil potential therapeutic targets. Here, we used proximity labeling to identify protein interactors of active KRAS in PDAC cells. We expressed fusions of wild-type (WT) (BirA-KRAS4B), mutant (BirA-KRAS4B^{G12D}), and nontransforming cytosolic double mutant (BirA-KRAS4B$^{G12D/C185S}$) KRAS with the BirA biotin ligase in murine PDAC cells. Mass spectrometry analysis revealed that RSK1 selectively interacts with membrane-bound KRAS^{G12D}, and we demonstrate that this interaction requires NF1 and SPRED2. We find that membrane RSK1 mediates negative feedback on WT RAS signaling and impedes the proliferation of pancreatic cancer cells upon the ablation of mutant KRAS. Our findings link NF1 to the membrane-localized functions of RSK1 and highlight a role for WT RAS signaling in promoting adaptive resistance to mutant KRAS-specific inhibitors in PDAC.

KRAS | PDAC | NF1 | BioID | RSK

A total of 60,430 new cases of pancreatic cancer were estimated for 2021, and the 5-y relative survival rate has consistently remained below 11% (1). About 85% of these pancreatic cancer tumors are pancreatic ductal adenocarcinoma (PDAC) (2). Poor outcomes of PDAC cases result from late diagnoses leading to unresectable and heterogeneous tumors as well as ineffective therapies, which only prolong survival on the order of months (3–5). Mutations in the KRAS proto-oncogene are present in over 90% of PDAC cases and are associated with a poor prognosis (6). Furthermore, mice expressing mutant KRAS in the pancreas develop precursor lesions, which sporadically progress into frank PDAC. This progression is accelerated when combined with other mutations or deletion of tumor suppressor genes (7–11). Additionally, independent studies have shown that the maintenance of murine PDAC cells require KRAS (12–14).

As a RAS GTPase, KRAS acts as a molecular switch at the plasma membrane that relays growth factor signaling from receptor tyrosine kinases to downstream pathways such as RAF/MEK and PI3K/AKT (15). GTP binding alters the conformation of the KRAS G domain, thereby creating binding sites for downstream effectors to trigger enzymatic cascades that promote cell transformation (16–19). Intrinsically, KRAS slowly hydrolyzes GTP into GDP to halt signaling; however, GTPase activating proteins (GAPs) such as neurofibromin 1(NF1) catalyze this process (20). In contrast, guanine nucleotide exchange factors, such as son of sevenless homolog 1 (SOS1), catalyze the exchange of GTP for bound GDP. In most PDAC cases, KRAS is mutated at the 12th residue located in the G domain from glycine to either a valine (G12V), or more commonly, aspartate (G12D). These mutations sterically prevent the "arginine finger domain" of GAPs from entering the GTPase site, thereby blocking extrinsic allosteric GTPase activation and stabilizing RAS-GTP (21, 22). Activating mutations in KRAS constitutively trigger RAF/MEK and PI3K/AKT pathways leading to increased cell proliferation as well as other prooncogenic behaviors (15). KRAS signaling not only relies on the G domain but also the C-terminal hypervariable domain (HVR), which is required to stabilize KRAS on membranes where signaling is most efficient (23–26). Independent studies suggest that specific biochemical and cellular consequences of KRAS activation are attributed to the unique properties of the HVR of the predominant splice form KRAS4B, namely the polybasic domain and the lipid anchor (27–30). Localization of RAS proteins to the plasma membrane requires the prenylation of the CAAX motif (23). Additionally, for KRAS4B, the hypervariable region contains a highly polybasic domain consisting of several consecutive lysines, which can interact with the negative charges on the polar heads of phospholipids and stabilize protein interactions (31). Structural and biochemical characterization of the HVR and G domain has contributed to a better understanding of the signaling outputs of KRAS and led to KRAS-targeting strategies.

Significance

For decades, KRAS interactors have been sought after as potential therapeutic targets in KRAS mutant cancers, especially pancreatic ductal adenocarcinoma (PDAC). Our proximity labeling screen with KRAS in PDAC cells highlights RSK1 as a notable mutant-specific interactor. Functionally, we show that RSK1 mediates negative feedback on wild-type (WT) KRAS in PDAC cells. Targeting oncogenic KRAS eliminates the negative feedback on WT RAS and highlights a role for WT RAS signaling in promoting adaptive resistance to mutant KRAS ablation.

Author contributions: D.K.C., T.E.O., L.V.A., and D.A.T. designed research; D.K.C., T.E.O., J.S.T., Y.P., H.-C.T., K.D.R., and D.J.P. performed research; D.K.C., T.E.O., Y.P., B.A., N.V.P., and K.A. contributed new reagents/analytic tools; D.K.C., T.E.O., J.S.T., Y.P., K.D.R., and D.J.P. analyzed data; and D.K.C., T.E.O., and D.A.T. wrote the paper.

Competing interest statement: D.A.T. is a member of the Scientific Advisory Board and receives stock options from Leap Therapeutics, Surface Oncology, and Cygnal Therapeutics. D.A.T. is cofounder of Mestag Therapeutics. D.A.T. receives grant funding from the Lustgarten Foundation. D.A.T. has received Sponsored Research Agreements from Fibrogen, Mestag, and ONO Therapeutics.

This article is a PNAS Direct Submission.

[1]D.K.C. and T.E.O. contributed equally to this work.

[2]To whom correspondence may be addressed. Email: dtuveson@cshl.edu.

This article contains supporting information online at https://www.pnas.org/lookup/suppl/doi:10.1073/pnas.2016904118/-/DCSupplemental.

Published May 21, 2021.

Various approaches to inhibit KRAS include direct inhibition, expression interference, mislocalization, and targeting of downstream effectors (32). Thus far, direct inhibitors against KRAS have only successfully targeted the G12C mutant, which comprises 2.9% of KRAS mutant PDAC (21, 33). For other KRAS mutants, targeting downstream effectors of KRAS in pancreatic cancer remains an alternative approach. Unfortunately, dual inhibition of MEK and AKT pathways was ineffective in PDAC patients (34). Difficulty in targeting KRAS due to adaptive resistance and feedback regulation motivates a better understanding of KRAS biology (35). For example, although PDAC typically features a mutant KRAS, there may be a role for its wild-type (WT) counterpart as well as WT RAS paralogs (HRAS and NRAS), which are GAP sensitive and subject to signaling feedback. While oncogenic KRAS has been shown to activate WT HRAS and NRAS via allosteric stimulation of SOS1 (36), WT KRAS has been proposed to be a tumor suppressor in some KRAS mutant cancers based on the commonly observed mutant-specific allele imbalance that occurs throughout tumor progression (37). Additionally, the reintroduction of WT KRAS abolished tumor T cell acute lymphoblastic leukemia development and impaired tumor growth in KRAS mutant lung cancer cells in vivo (37–39). The discovery of novel KRAS protein interactors involved in downstream signaling or feedback and compensatory pathways may elucidate why inhibition of downstream pathways have had limited clinical impact in PDAC. Here, we perform proximity labeling experiments by expressing a fusion of $BirA^{R118G}$ biotin ligase and KRAS in PDAC cells, which, in the presence of high concentrations of biotin, generates reactive biotinoyl-AMP that labels lysines of nearby proteins, such as interactors of its fusion partner KRAS (40–42). The biotinylated interactor proteins can be isolated by streptavidin pulldown and analyzed by proteomics to identify novel protein interactors (43–45). Because covalent labeling occurs in living cells, enzymatic labeling may potentially identify transient interactors and protein complexes.

Two recent studies used proximity-dependent biotin identification (BioID) labeling methods to identify KRAS interactors in 293T and colon cancer cells (46, 47). These studies uncovered and validated the functional relevance of PIP5KA1 and mTORC2 in PDAC cells. However, BirA-KRAS screens in PDAC models have not yet been performed. Since the tumor context may determine protein expression and relevant interactions, we sought to perform a BirA-KRAS screen in PDAC cells. We hypothesize that proximity labeling with BioID presents a means for identifying new mutant KRAS-specific interactions in PDAC, which may unveil new insights into therapeutic design for this malignancy.

Results

BioID-KRAS in Pancreatic Ductal Adenocarcinoma Cells. To identify interactors of mutant KRAS in PDAC and better understand mutant KRAS biology, we performed BioID screening in mouse PDAC cells. Notably, our studies focused on using BioID with $KRAS^{G12D}$, the most common mutation in PDAC. To label proteins proximal to KRAS in PDAC cells, we designed and expressed various BioID fusion proteins with BirA and KRAS4B, the ubiquitously expressed *Kras* splice isoform (Fig. 1*A*) (28). We fused both mutant ($Kras^{G12D}$) and WT murine *Kras* ($Kras^{WT}$) to the C terminus of myc-tagged *BirA* to create *BirA-*$Kras^{G12D}$ (B-G12D) and *BirA-*$Kras^{WT}$ (B-WT). Since the polybasic domain and CAAX motif at the C-terminal are both required for the membrane localization of KRAS, we designed a membrane-localized BirA control (B-CAAX) by fusing the last 20 amino acids of murine KRAS to BirA (48, 49). As the signaling and biological function of KRAS depend on its membrane localization (50, 51), we sought to identify membrane-specific $KRAS^{G12D}$ interactors by creating a double mutant BirA-KRAS fusion protein, which harbors an additional mutation in the CAAX motif (B-G12D/C185S), as a nontransforming cytosolic comparator. To make the screen relevant to PDAC, we performed the experiment in three cell lines (mT42, mT93, and mT95) derived from *FRT-LSL-*$Kras^{G12V}$*-FRT; LSL-*$Trp53^{R172H}$*; Pdx1-Cre;R26-FlpOERT2* (FPC) mouse PDAC tumors (*SI Appendix*, Fig. S1*A*) (52). The endogenous expression of $KRAS^{G12V}$ in this mouse model and isolated cell lines is distinguishable from our exogenously expressed BirA-$KRAS^{G12D}$ by mass spectrometry (MS) and can be excised upon 4-hydroxy-tamoxifen (4-OHT) treatment. This minimizes competition from the endogenous mutant KRAS that may confound the identification of BirA-KRAS interactors.

We first validated the localization of our panel of B-WT, B-G12D, B-CAAX, and B-G12D/C185S proteins in mT42 FPC cells by isolating membrane and cytoplasmic fractions using sequential fractionation (53). As expected, B-WT, B-G12D, and B-CAAX proteins localized to the membrane, whereas the CAAX mutant B-G12D/C185S localized to the cytoplasm (Fig. 1*B*). We validated these findings by myc-tag immunofluorescence stains of B-WT, B-G12D, and B-CAAX proteins, which displayed plasma membrane localization, and B-G12D/C185S protein, which was predominantly cytosolic in PDAC cells (Fig. 1*C*). Together, these experiments demonstrate the appropriate localization of the various fusion constructs.

To ensure that these BirA fusion proteins were functional, we performed Western blotting analyses of RAS effector pathways in 293T and 3T3 cells expressing these constructs. Expectedly, only B-G12D activated RAS effector pathways, ERK and AKT, in HEK293T and 3T3 cells, respectively (*SI Appendix*, Fig. S1 *B* and *C*). Additionally, among the BirA-KRAS fusion proteins, B-G12D was the most potent stimulator of cell proliferation and exclusively conferred anchorage-independent growth in 3T3 cells (*SI Appendix*, Fig. S1 *D* and *E*). To determine the functionality of the BirA ligase, we infected FPC cells to express the B-WT, B-G12D, B-CAAX, and B-G12D/C185S fusion constructs and treated the cells with biotin to determine whether the known RAS interactor RAF1 would be preferentially biotinylated by any of these fusion proteins. Indeed, B-G12D preferentially biotinylated more RAF1 than B-WT and B-CAAX but biotinylated comparable levels of RAF1 as B-G12D/C185S (Fig. 1*D*). This finding suggests that the interaction of RAF1 with KRAS depends on the GTP-bound state of KRAS rather than its localization and does not necessarily cause RAS pathway activation as has been previously reported (54). We also assessed the functional properties of these BirA constructs in FPC cells with and without the excision of the endogenous mutant KRAS. We found that steady-state activation of ERK and AKT pathways were not markedly altered in mT42 cells stably expressing these constructs (*SI Appendix*, Fig. S1*F*), suggesting the establishment of feedback loops. We also found that the expression levels of BirA-KRAS fusion proteins were comparable to or less than endogenous KRAS levels. Nonetheless, B-G12D increased proliferation and restored colony formation after $Kras^{G12V}$ excision in mT93 FPC cells (*SI Appendix*, Fig. S1 *G* and *H*). These results provide additional evidence that the BirA-$KRAS^{G12D}$ fusion retains oncogenic properties and that proximity labeling using these constructs could identify functionally relevant interactors.

Having characterized the functional aspects of our BirA-KRAS fusion proteins, we sought to compare our KRAS proximity labeling approach to the standard immunoprecipitation approach for identifying protein interactors of KRAS. To this end, we harvested protein lysate from biotin-treated B-WT– and B-G12D–expressing FPC cells and simultaneously performed a streptavidin pulldown and immunoprecipitation followed by Western blot analysis. Given the same input amount and conditions, both approaches were able to detect similar amounts of RAF1, whereas streptavidin pulldown was superior in detecting the p110-α subunit of PI3-Kinase

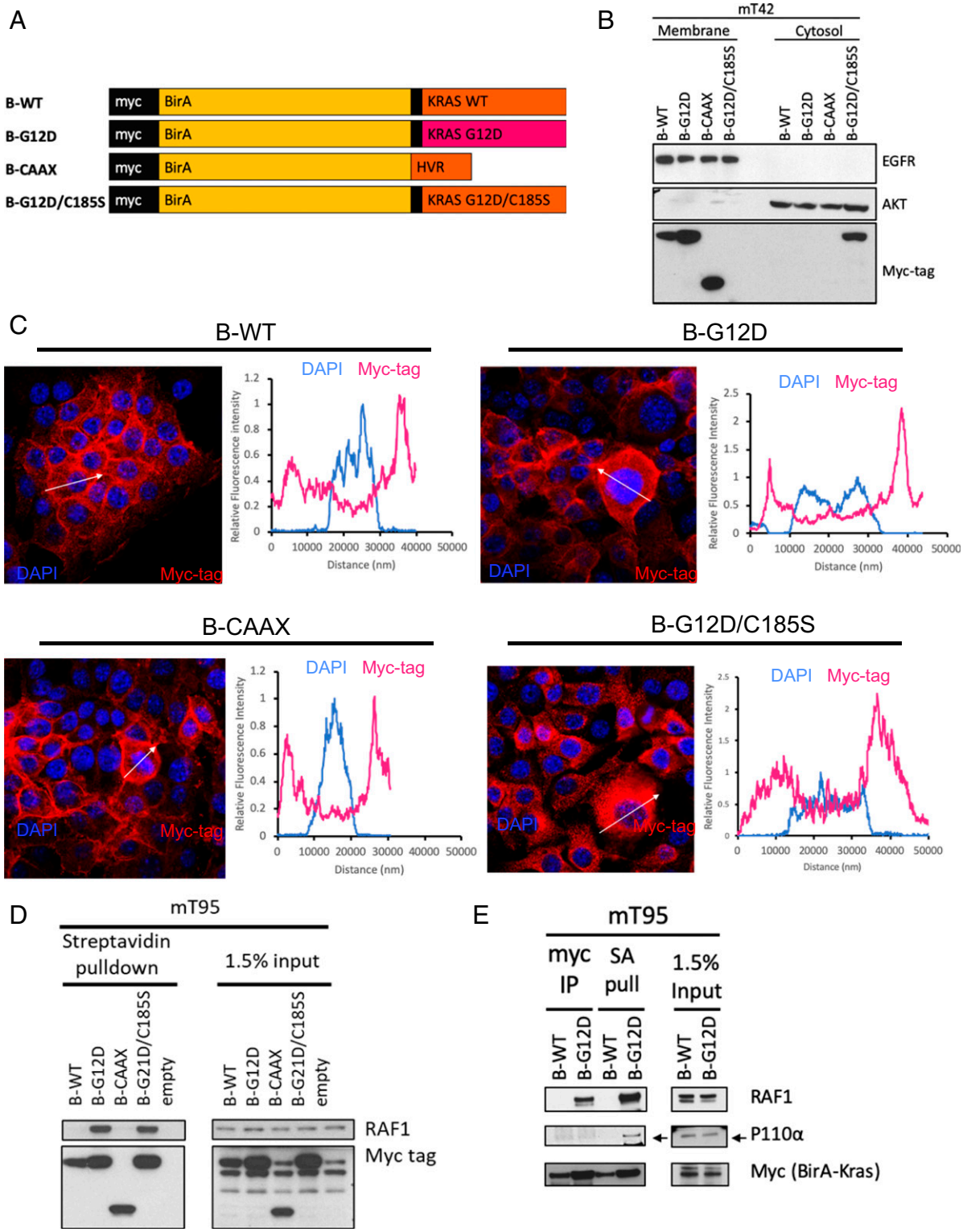

Fig. 1. Properties of BirA-KRAS fusions. (*A*) Design of BirA-KRAS fusion constructs. Myc-tagged BirA was fused to the N terminus of murine WT KRAS4B or mutant KRAS4BG12D with a short glycine linker (GGSG). Membrane-localized BirA was created by fusing the last 20 amino acids of murine KRAS to myc-tagged BirA. KRAS4BG12D/C185S was created by mutating the cysteine residue in the CAAX prenylation motif to mislocalize the protein. (*B*) mT42-2D cells expressing B-WT, B-G12D, B-CAAX, and B-G12D/C185S were sequentially fractionated into cytosolic and membrane isolations and probed for myc-tag, as well as EGFR and AKT representing membrane and cytosolic controls, respectively. (*C*) Immunofluorescence (IF) of B-WT, B-G12D, B-CAAX, and B-G12D/C185S in mT93-2D cells. Staining of the myc-tagged BirA fusions are represented in red while DAPI-stained nuclei are represented in blue in the IF images. The arrows indicate the profiles taken for the relative fluorescent intensities from one edge to the other edge in cells (adjacent panels). (*D*) mT95-2D FPC cells were infected to express B-WT, B-G12D, B-CAAX, B-G12D/C185S, or empty control. Cells were incubated with 50 μM biotin for 24 h prior to lysis and streptavidin pulldown. Elutions and 1.5% input were probed for RAF1 and myc-tag BirA. (*E*) Lysate from mT95 expressing B-WT and B-G12D was used for both immunoprecipitation (IP) and streptavidin (SA) pulldown under similar lysis and washing conditions and probed for RAF1, p110-α, and the myc-tagged BirA-Kras fusions.

(Fig. 1*E*). Stoichiometry may limit the immunoprecipitation approach such that only a fraction of enriched B-G12D molecules coprecipitates p110-α; however, in the proximity labeling approach, a single molecule of B-G12D may biotinylate several molecules of p110-α, increasing its detection by streptavidin pulldown. Because BioID was more sensitive in detecting the interaction of p110-α with KRAS than immunoprecipitation, we set out to employ this approach to identify interactors by MS.

Proximity Labeling Identifies RSK1 as a Mutant- and Membrane-Specific KRAS Interactor. To detect interactors of oncogenic KRAS, we performed BioID-MS analysis on three biological replicates of murine FPC tumor cells (mT42, mT93, and mT95). For each parental cell line, we generated cell lines stably expressing each of our BioID constructs (B-WT, B-G12D, B-CAAX, and B-G12D/C185S). The comparison of B-G12D to B-WT and/or B-G12D to B-G12D/C185S would enable the detection of mutant-specific and/or membrane-specific interactors, respectively (Fig. 2*A*). To determine whether endogenous mutant $KRAS^{G12V}$ could affect the interactors identified, these cells were treated with 4-OHT to ablate the expression of $Kras^{G12V}$ or dimethyl sulfoxide (DMSO) as a vehicle control for 3 d prior to biotin treatment, followed by lysate harvest, streptavidin pulldown, and MS analysis. To account for differences in BirA expression in each cell line and the variability in the number of peptides in each run for MS, we normalized the quantitative peptide abundance to the BirA counts for each experiment.

Several observed peptides validated this approach for both the vehicle-treated (Fig. 2*B*) and 4-OHT–treated cells (*SI Appendix*, Fig. S2*A*). MS detected shared KRAS peptides and also identified the G12-containing peptide across the three full-length BirA-KRAS variants. Interestingly, G12V peptides were not found in any of the samples run, suggesting that either the BirA tag prevents $KRAS^{G12D}$:$KRAS^{G12V}$ dimer formation or that such heterodimers may be too scarce to detect. Additionally, samples with an intact CAAX box enriched for membrane-localized proteins, such as FAM129B (also known as niban-like protein 1 or MINERVA), compared to samples from cytosolic B-G12D/C185S. B-G12D and B-G12D/C185S had similar biotinylation levels of RAF1, whereas B-WT and B-CAAX labeled less RAF1, consistent with our Western blot results (Fig. 1*D*).

To identify $KRAS^{G12D}$ effectors, we compared the proteins enriched by B-G12D and B-WT from our BioID-MS experiments and nominated 91 protein matches that met the criteria of being enriched in at least two out of three biological replicates in the setting of the endogenous mutant $Kras^{G12V}$ allele. To further prioritize this list, we also queried for membrane-specific candidates identified by comparing B-G12D to B-G12D/C185S and found 255 proteins in at least two out of three biological replicates. Among them, 66 candidate proteins were both mutant specific and membrane specific (*SI Appendix*, Table S1 and Fig. S2*B*). Interestingly, when sorted by membrane enrichment, ARAF was preferentially biotinylated at the membrane whereas RAF1 and BRAF were both comparably labeled by B-G12D and B-G12D/C185S (*SI Appendix*, Table S2 and Fig. S2*C*). Although the direct interaction of KRAS and ARAF is well established, these data suggest that our approach could map spatially distinct proximal interactors and uncover dynamic $KRAS^{G12D}$ interactors on the membrane.

To further refine our list and prevent confounding effects of endogenous mutant KRAS due to competition for substrates, we also performed BioID-MS analysis on the same BirA-KRAS–expressing FPC cells treated with 4-OHT to excise the endogenous mutant $Kras^{G12V}$ allele (*SI Appendix*, Fig. S2*D*). By prioritizing candidates that were nominated in the mutant-specific and membrane-specific comparison for both the vehicle and 4-OHT conditions, we further narrowed our list to 32 proteins (Fig. 2*C*). Of these proteins, 11 matches were known interactors or KRAS effectors, including RAF family members (ARAF, BRAF, and RAF1), SPRED1, SPRED2, NF1, MLLT4, RIN1, and mTORC2 complex members (MAPKAP1, RICTOR, and DEPTOR) (Fig. 2*D* and *SI Appendix*, Table S3). Of the remaining 21 candidates, PLEKHA2, MYO1E, and RPS6KA1 (RSK1) were also enriched in the B-G12D to B-WT comparison as previously reported in BioID screens in HEK293 cells (47, 55). Several known RAS interactors, including PI3K, KSR, RALBP, SOS1, and PIP5KA1, were not detected in our MS data set, suggesting that additional approaches may be needed to increase the sensitivity of BioID assay in PDAC cells. Nonetheless, ARAF and RSK1 were the most consistently enriched candidates in the B-G12D to B-WT comparison in the 4-OHT setting.

Of the interactors that were nominated to be both $KRAS^{G12D}$ specific and plasma membrane localized, RICTOR, ARAF, and RSK1 were among those validated by Western blot analysis of the BioID samples (Fig. 2*E*). To validate the RSK1–KRAS interaction and determine whether it is stable and therefore amenable to immunoprecipitation, we performed myc-tag coimmunoprecipitation in parallel with streptavidin pulldown of lysates from FPC cells expressing either B-WT or B-G12D. Unlike ARAF, RSK1 was only detected by streptavidin pulldown of B-G12D samples and failed to appreciably enrich by immunoprecipitation (Fig. 2*F* and *SI Appendix*, Fig. S2*E*), suggesting that the RSK1–$KRAS^{G12D}$ interaction is transient, weak, or indirect.

NF1 Recruits RSK1 to the Oncogenic KRAS Interactome. Unlike RAFs and the mTORC2 complex, RSK1 lacks a known RAS-binding domain (RBD). Therefore, we reasoned that the proximity of RSK1 to oncogenic KRAS may depend upon another protein in murine PDAC cells, similar to the dependency of RICTOR on MAPKAP1 for proximity to KRAS (47). To test this hypothesis, we employed both BioID and CRISPR/Cas9 knockout (KO) approaches. BioID enables the detection of transient or weak $KRAS^{G12D}$ interactors, which are difficult to identify by immunoprecipitation, whereas the selective ablation of proteins in the $KRAS^{G12D}$ biotinylated interactome enables the identification of proteins that promote the proximity of RSK1 to $KRAS^{G12D}$ on the membrane. Accordingly, we investigated whether ablating membrane-specific proximal interactors of B-G12D, such as MAPKAP1, RICTOR, and NF1, would abolish the proximity biotinylation of RSK1 by B-G12D in mT42 and mT93 cells. As expected, MAPKAP1 KO decreased the $KRAS^{G12D}$-mediated biotinylation of RICTOR; however, the depletion of neither mTORC2 component decreased RSK1 biotinylation (Fig. 3*A*). Interestingly, only NF1 depletion abrogated RSK1 biotinylation, suggesting that NF1 selectively mediates RSK1 interaction with oncogenic KRAS (*SI Appendix*, Fig. S3 *A* and *B*). Since NF1 loss promotes WT RAS activation, competition for RSK1 between WT RAS and mutant KRAS could provide an alternative explanation for the decreased RSK1–$KRAS^{G12D}$ interaction upon NF1 KO. To exclude this possibility, we excised the endogenous mutant KRAS in FPC cells expressing either B-G12D or B-WT and then ablated *Nf1* with CRISPR/Cas9. We hypothesized that if WT KRAS could compete for RSK1 binding, then the complete ablation of oncogenic KRAS in B-WT–expressing cells would lead to elevated RSK1 biotinylation. On the contrary, we found that RSK1 was biotinylated in B-G12D but not B-WT–expressing cells (*SI Appendix*, Fig. S3*B*), suggesting that the decrease in RSK1–$KRAS^{G12D}$ interaction upon NF1 loss cannot be explained by WT KRAS activation. Since RSK1 requires NF1 to interact with $KRAS^{G12D}$ on the membrane, and SPRED proteins are essential for the membrane recruitment of NF1 to the RAS interactome (56, 57), we tested whether KO of *Spred1* and *Spred2* would decrease the RSK1–$KRAS^{G12D}$ interaction, measured by RSK1 biotinylation.

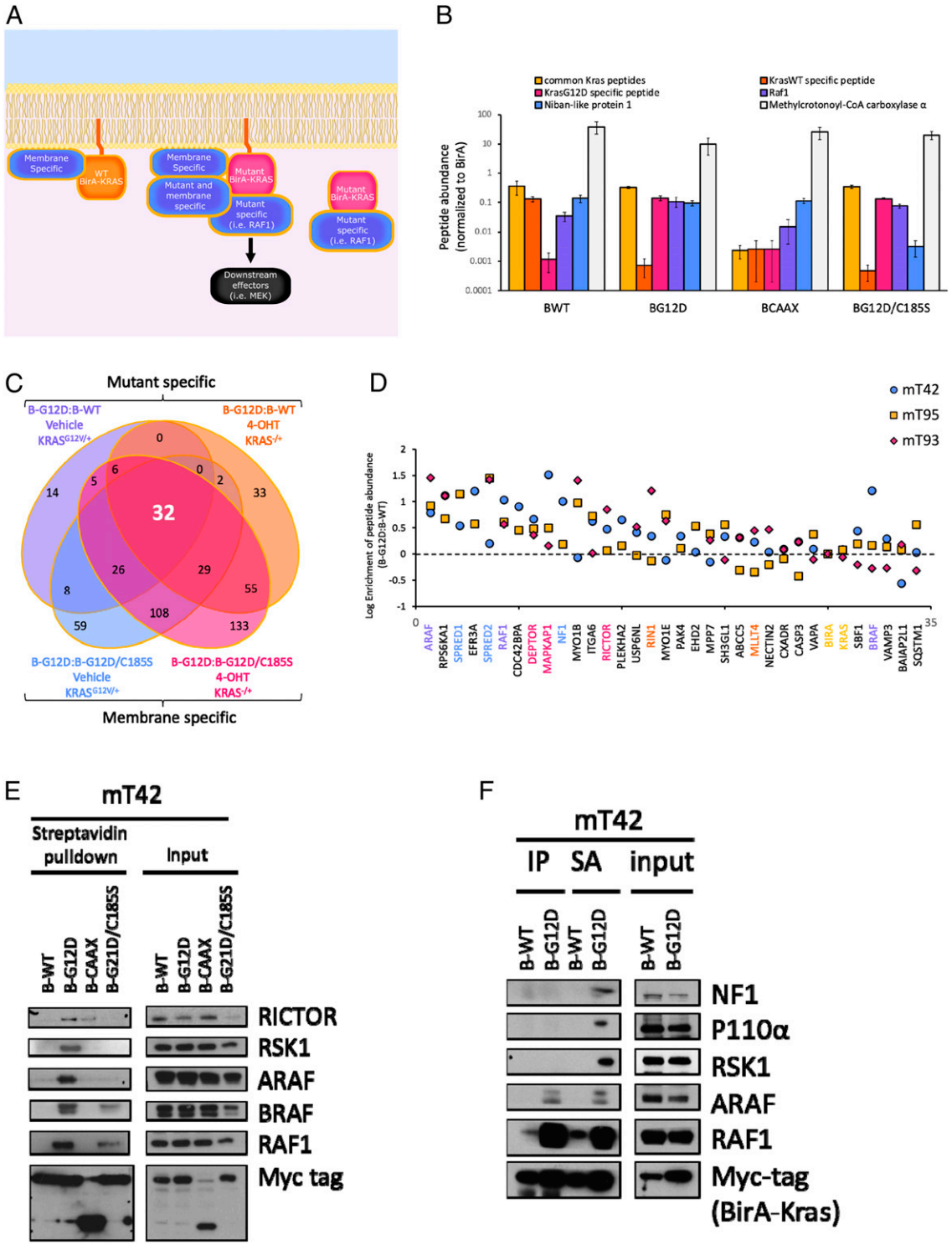

Fig. 2. Proximity labeling nominates RSK1 as a mutant- and membrane-specific KRAS interactor. (*A*) Schematic of the method for determining mutant-specific interaction by comparing B-G12D to B-WT and membrane-specific interactions by comparing B-G12D to B-G12D/C185S. (*B*) MS relative quantification of internal control KRAS peptides and positive controls (RAF1 and niban-like 1) after normalization to BirA counts for B-WT, B-G12D, B-CAAX, and B-G12D/C185S samples from vehicle-treated FPC cells. Error bars represent SEM ($n = 3$). (*C*) Venn diagram of the overlap of candidates that met the criteria for being mutant specific and membrane specific in both the 4-OHT–treated and control-treated conditions for two out of three biological replicates. The 32 candidates met all criteria. (*D*) Enrichment of peptide abundances for the 32 candidate interactors as well as KRAS and BirA control peptides. Known KRAS interactors include RAF members (purple), NF1/SPRED proteins (blue), mTORC2 (magenta), and RBD-containing proteins (orange) with the internal controls BirA and KRAS (yellow). Enrichment is plotted on a scale of log base 10. (*E*) BioID was performed on mT42 expressing B-WT, B-G12D, B-CAAX, or B-G12D/C185S followed by Western blot analysis to confirm RICTOR, RSK1, ARAF, BRAF, and RAF1 as B-G12D substrates. (*F*) mT42 cells expressing B-WT and B-G12D were treated with 50 μM biotin for 24 h and harvested in HEPES-based Nonidet P-40 lysis buffer. Lysates were either incubated for 4 h with streptavidin (SA) beads or 3 h with myc-tag antibody followed by 1 h with protein G Dynabeads to compare the performance of BioID to coimmunoprecipitation. SA pulldowns and immunoprecipitations (IPs) were analyzed by Western blot for the detection of NF1, p110-α, RSK1, ARAF, RAF1, and myc-tag.

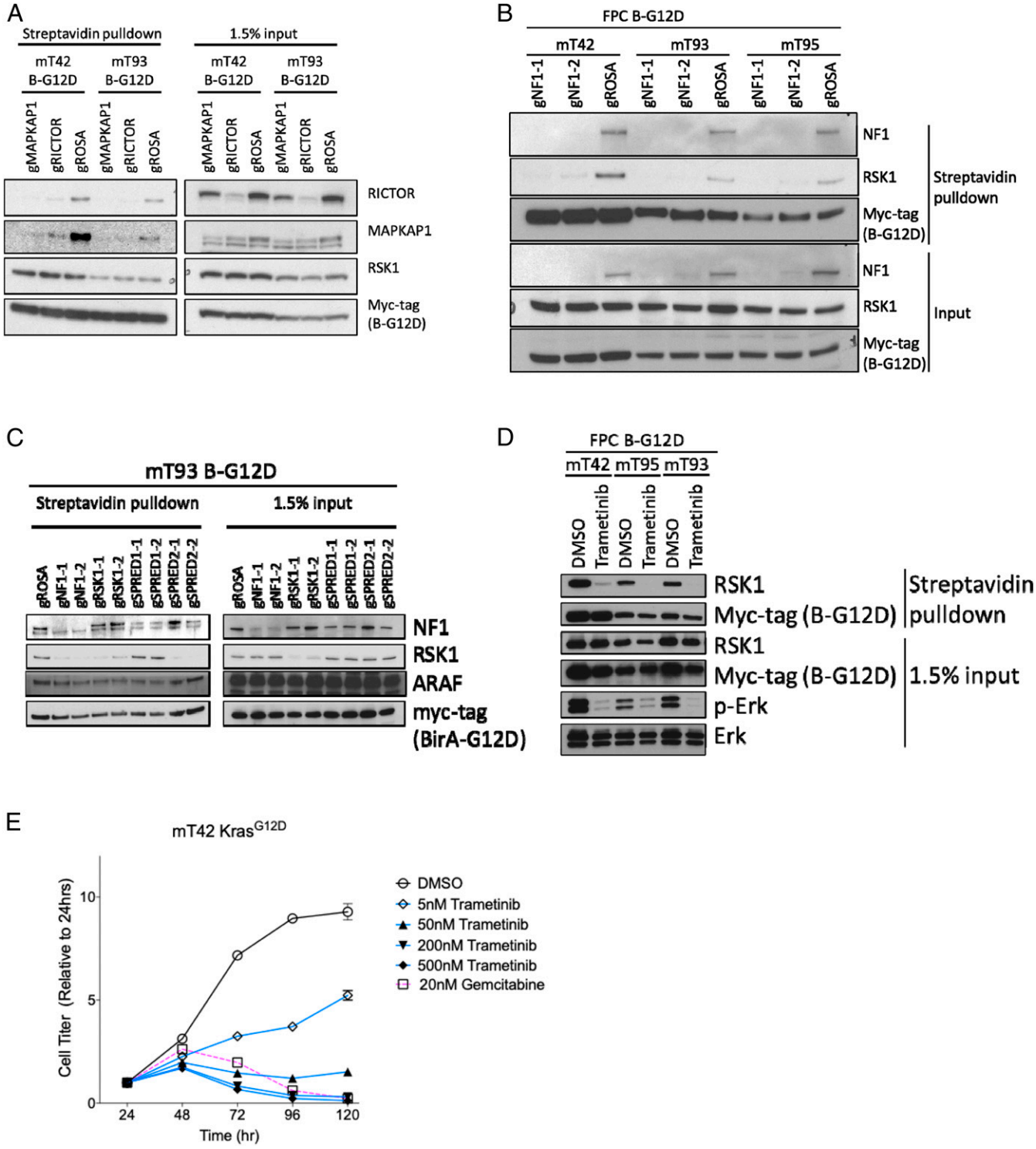

Fig. 3. NF1 recruits RSK1 to the oncogenic KRAS interactome. (*A*) BioID of mT42 and mT93 expressing B-G12D with CRISPR depletion of MAPKAP1 and RICTOR were analyzed by Western blot to detect the biotinylation of these mTORC2 components by B-G12D. (*B*) BioID of mT42, mT93, and mT95 expressing B-G12D with CRISPR depletion of NF1. (*C*) BioID of mT93 expressing B-G12D with CRISPR depletion of NF1, RSK1, SPRED1, and SPRED2. (*D*) FPC cell lines expressing B-G12D were treated with 500 nM trametinib during the 24 h biotin incubation. The lysates and streptavidin pulldown were analyzed for the presence of RSK1, NF1, ARAF, and myc-tag as well as the phosphorylation status of MAPK. (*E*) The 5-d cell proliferation curves of mT42 cells expressing B-G12D treated with 5, 50, 200, 500 nM trametinib were compared to negative control DMSO and positive control gemcitabine.

Although we could not confirm SPRED2 depletion at the protein level due to the lack of suitable antibodies, we validated successful gene editing at the target sites of both guide RNAs against *Spred2* (*SI Appendix*, Fig. S3*C*). Whereas guides directed against *Spred1* slightly decreased NF1 biotinylation, *Spred2* but not *Spred1* depletion abolished RSK1 biotinylation (Fig. 3*C* and *SI Appendix*, Fig. S3*D*), suggesting that a SPRED2/NF1 membrane complex bridges the interaction between RSK1 and oncogenic KRAS. In line with a

mutant KRAS interactome comprising RSK1, SPRED2, and NF1, these proteins were nominated as the top 13th, 14th, and 20th interactors specific to $KRAS^{Q61H}$ in the human cell map dataset (55). Taken together, our results demonstrate that the proximity of RSK1 to $KRAS^{G12D}$ depends on NF1 and SPRED2 and suggest a function for these negative regulators of RAS signaling.

RSK1 to 4 are a family of serine/threonine kinases known to be activated by ERK signaling and translocated to the plasma membrane transiently and in an ERK-dependent manner upon EGF stimulation (58, 59). To test whether MEK/ERK pathway activation regulates the interaction between RSK1 and mutant KRAS, we treated B-G12D–expressing FPC cells with 500 nM of the MEK inhibitor trametinib or vehicle control during the biotin incubation of the BioID assay and performed streptavidin pulldown and Western blot for RSK1. MEK inhibition markedly decreased phospho-ERK levels and abrogated RSK1 biotinylation by B-G12D (Fig. 3*D*), suggesting that the RSK1–$KRAS^{G12D}$ interaction depends on MEK/ERK pathway activation. To determine whether the abrogation of $KRAS^{G12D}$-mediated RSK1 biotinylation is a secondary effect of suppressing cellular proliferation rather than a specific effect of inhibiting the MEK/ERK pathway, we evaluated the proliferation of mT42 G12D-expressing cells upon treatment with 20 nM gemcitabine, a cytotoxic drug, or 5, 50, 200, and 500 nM trametinib. As expected, gemcitabine suppressed the proliferation of these cells. Similarly, trametinib inhibited their proliferation in a concentration-dependent manner (Fig. 3*E*). Having confirmed the effects of these drugs on cellular proliferation, we repeated the BioID experiment with increasing doses of trametinib, vehicle control, or 20 nM gemcitabine. Western blot analyses confirmed the loss of RSK1 biotinylation upon the inhibition of ERK activation, whereas RSK1 biotinylation was mostly unchanged in gemcitabine-treated cells (*SI Appendix*, Fig. S3*E*), thereby confirming that the loss of RSK1 biotinylation upon MEK inhibition is a direct consequence of MEK/ERK pathway inhibition. Since ERK-mediated phosphorylation of RSK1 has been previously linked to its membrane translocation (59), we sought to determine whether a decrease in RSK phosphorylation by ERK could explain the loss of RSK1 biotinylation upon MEK inhibition.

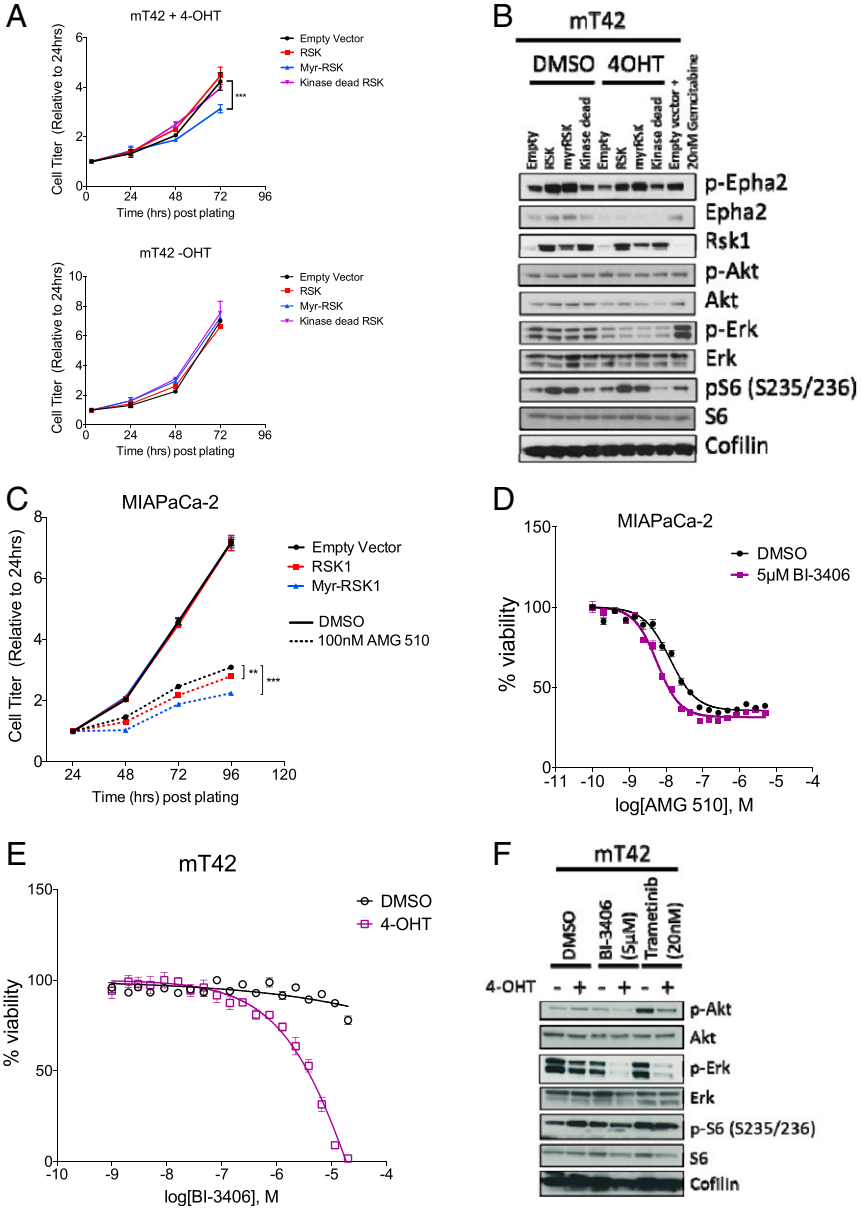

Fig. 4. Membrane-localized RSK1 exerts negative feedback on WT RAS. (*A*) FPC cell line mT42 cells ectopically expressing RSK1, myr-RSK1, or empty vector control were plated for cell proliferation and treated with DMSO or 4-OHT, then measured by CellTiter-Glo luminescence assay every day for 4 d. (*B*) mT42 FPC cells ectopically expressing RSK1, myr-RSK1, or empty vector control were treated with DMSO or 4-OHT and analyzed by Western blot. Gemcitabine was used as a proliferation control. Immunoblotting was performed for RSK1 with RAS pathways represented by phospho-ERK and phospho-AKT, and the RSK1 substrates, phospho-EPHA2 and phospho-S6. (*C*) MIA PaCa-2 cells expressing RSK1, myr-tag RSK1, and empty vector control were seeded at 2,000 cells per well and treated with either 100 nM AMG 510 or DMSO control, then measured by CellTiter-Glo luminescence assay every day for 4 d. (*D*) MIA PaCa-2 cells were seeded at 2,000 cells per well and treated 24 h after seeding with 5 μM BI-3406 or DMSO control and AMG 510 (from 5 μM to 0.1 nM). Cell viability was measured after 4 d with CellTiter-Glo. (*E*) mT42 cells were seeded at 1,000 cells per well and treated with 4-OHT or DMSO control and BI-3406 in a dose–response manner (from 20 μM to 2 nM). Cell viability was measured using CellTiter-Glo Luminescence assay at day 4. (*F*) FPC cell line mT42 cells were treated with 5 μM BI-3406, 20 nM trametinib, or DMSO vehicle control in the presence or absence of mutant KRAS by treatment with DMSO vehicle control or 4-OHT, respectively. Immunoblotting was performed for RAS pathways by phospho-ERK and phospho-AKT and the RSK1 substrate phospho-S6.

To this end, we treated mT42 cells with 50 nM trametinib and performed Western blot analysis for phospho-RSK (S380). Phospho-RSK decreased upon MEK inhibition, supporting a model in which MEK/ERK pathway inhibition reduces RSK phosphorylation and regulates its ability to interact with NF1 (*SI Appendix*, Fig. S3*F*). Since ERK activation induces the expression of negative regulators of the RAS pathway, including SPRED, SPROUTY, and DUSP family proteins, we asked whether ERK deactivation via MEK inhibition decreases SPRED1/2 expression, thereby preventing the membrane localization and recruitment of the NF1/RSK1 complex to the mutant KRAS interactome. Indeed, we found that DUSP6, SPRED1, and SPRED2 were all potently down-regulated following MEK inhibition in mT42 FPC cells in a time- and concentration-dependent manner (*SI Appendix*, Fig. S3*G*), providing an additional explanation for the loss of RSK1 biotinylation by oncogenic KRAS in the context of MEK inhibition.

Membrane-Localized RSK1 Exerts Negative Feedback on WT RAS. Having established an active KRAS interactome including NF1 and RSK1, we sought to determine a functional role for membrane-localized RSK1 in PDAC cells. RSK1 is a known ERK pathway effector, and membrane-targeted RSK1, considered to be constitutively active, can confer MEK independence and mediate pro-survival signals in IL-3–dependent cells (60). However, in other cellular contexts, membrane-localized RSK1 has also been shown to inhibit RAS signaling (61). As KRAS localizes to the plasma membrane, we used a myristoylation (myr) tag to target RSK1 to the plasma membrane (62) (*SI Appendix*, Fig. S4*A*). To identify whether membrane-targeted RSK1 regulates the RAS pathway or contributes to RAS-mediated transformation in PDAC cells, we retrovirally introduced RSK1 or myr-tagged RSK1 into parental mT42 cells and derivative cell lines stably expressing our tagged KRAS variants, B-WT, B-G12D, and B-G12D/C185S. For comparison, we also included overexpression of ARAF and myr-tagged ARAF as well as an empty vector control. These cells were plated sparsely and treated with 4-OHT for 3 d to excise endogenous $Kras^{G12V}$ before crystal violet staining to measure foci formation. Expectedly, mT42 cells expressing B-G12D formed colonies normally despite the removal of endogenous $Kras^{G12V}$, whereas the parental cells and cells with overexpression of B-WT and B-G12D/C185S were unable to rescue this loss and therefore exhibited less colonies (*SI Appendix*, Fig. S4 *B–D*). Myr-tagged ARAF, but not untagged ARAF, was able to partially rescue the loss of $KRAS^{G12V}$, consistent with the observation that membrane-targeted ARAF does not require active KRAS to activate downstream signaling (63). In contrast, myr-RSK1 further inhibited colony formation of mT42 parental cells and cells with either B-WT or B-G12D/C185S following the excision of $Kras^{G12V}$. Similarly, compared to empty vector, RSK1, or kinase-dead RSK1 expression, myr-RSK1 expression in mT42 FPC cells markedly attenuated proliferation following $Kras^{G12V}$ excision (Fig. 4*A*, *Top*) but had no effect on cellular fitness when endogenous $Kras^{G12V}$ was present (Fig. 4*A*, *Bottom*). We further validated this finding in mT93 cells (*SI Appendix*, Fig. S4*E*) and then sought to dissect the molecular underpinnings of this finding. Since membrane-targeted RSK produces a growth suppression phenotype only in cells lacking oncogenic KRAS, we hypothesized that this phenotype depends on the inhibition of WT RAS signaling.

To determine whether membrane-targeted RSK1 suppresses cellular proliferation by inhibiting the RAS pathway, we introduced empty vector, RSK1, kinase-dead RSK1, or myr-RSK1 to mT42 cells and treated the cells with either 4-OHT or DMSO control. We confirmed that these constructs were correctly expressed and functional by immunoblotting (Fig. 4*B*). As expected, cells expressing RSK1 or myr-RSK1 showed increased activation of RSK1 substrates such as S6 and EPHA2. There were no notable differences in the phosphorylation levels of ERK and AKT in the presence of endogenous mutant KRAS. However, upon mutant KRAS abrogation, phospho-ERK levels were markedly reduced in myr-RSK1 compared to kinase-dead RSK1 and empty vector–expressing cells. Importantly, mT42 empty vector–expressing cells treated with 20 nM gemcitabine exhibited no attenuation of ERK activation, indicating that the reduction of RAS signaling induced by myr-RSK1 is not a consequence of reduced proliferation. We also performed these experiments in mT93 cells and obtained similar results (*SI Appendix*, Fig. S4*F*). Collectively, these findings suggest that membrane-targeted RSK1 selectively exerts negative feedback on WT RAS signaling.

To extend these findings to human PDAC, RSK1 and myr-RSK1 were ectopically expressed in MIA PaCa-2 cells, which harbor a $KRAS^{G12C}$ mutation that can be targeted by the commercially available $KRAS^{G12C}$-specific inhibitor AMG 510 (64). To test whether membrane-localized RSK1 might affect cell proliferation as a function of the observed changes in RAS signaling pathways, we cultured RSK1-, myr-RSK1-, or empty vector–expressing MIA PaCa-2 cells with DMSO or 100 nM AMG 510. Whereas overexpression of RSK1 and myr-RSK1 had no effect on the proliferation of mT42 cells treated with DMSO, cells expressing these constructs, particularly myr-RSK1, exhibited increased sensitivity to 100 nM AMG 510 (Fig. 4*C*). To further validate these results using various concentrations of AMG 510, we performed dose curves in MIA PaCa-2 cells expressing empty vector, RSK1, and myr-RSK1 and similarly found that the blockade of oncogenic KRAS with AMG 510 sensitized these cells to RSK1 and myr-RSK–induced growth suppression (*SI Appendix*, Fig. S4*G*). This effect could not be induced by 20 nM gemcitabine (*SI Appendix*, Fig. S4*H*, *Top*), suggesting that AMG 510 elicits RSK1-mediated growth suppression through the blockade of oncogenic RAS pathway, rather than through its secondary effects on cellular fitness. To determine whether the attenuation of effector pathways downstream of oncogenic KRAS modulates the sensitivity to RSK1 expression, we treated MIA PaCa-2 cells expressing control and RSK constructs with 20 nM trametinib and performed proliferation assays. Interestingly, myr-RSK1 but not untagged RSK1 reduced proliferation following trametinib treatment (*SI Appendix*, Fig. S4*H*, *Bottom*). As the growth-suppressive effect of RSK1 occurs exclusively at the membrane, and membrane-targeted but not untagged RSK1 can bypass cellular control of its membrane localization, this result suggests that direct MEK inhibition has a greater effect on preventing RSK1 membrane localization compared to upstream oncogenic KRAS inhibition. Next, we sought to confirm whether membrane RSK1 inhibits RAS effector pathways following oncogenic KRAS blockade in MIA PaCa-2 cells in a similar manner to our prior findings in FPC cells. To this end, we treated MIA PaCa-2 cells expressing control and RSK constructs with 100 nM AMG 510 and harvested protein lysates for Western blot analyses at 1 h, 1 d, and 3 d after drug treatment. Remarkably, RSK1 and myr-RSK1 attenuated ERK activation especially following 1 d of AMG 510 treatment (*SI Appendix*, Fig. S4*I*). These findings nominate RSK1 as an interactor of mutant KRAS that bridges the downstream activation of ERK signaling to the upstream negative regulator of WT RAS, NF1. This suggests that RSK1/NF1 participates as a dual negative feedback inhibitor of WT RAS, consistent with previously described RSK1-mediated negative feedback that involves NF1 (65) and SOS1 (61). The resistance of PDAC cells to membrane-targeted RSK1 may reflect the indifference of oncogenic KRAS to NF1 GAP activity and less dependence on SOS1-mediated GTP loading compared to WT RAS.

Given the specificity of membrane RSK1 to WT RAS and because RSK1 has been previously shown to feedback inhibit

RAS/ERK signaling through the inhibition of SOS1 or through its activation of NF1 (61), we asked whether WT RAS inhibition through selective pharmacological inhibition of SOS1 could phenocopy the effects of membrane-targeted RSK. Accordingly, we treated MIA PaCa-2 cells with a combination AMG 510, to abrogate oncogenic KRAS signaling, and a selective SOS1 inhibitor, BI-3406, to block WT RAS signaling. Although MIA PaCa-2 cells have undergone loss of heterozygosity and do not possess WT KRAS, this cell line expresses other RAS isoforms, HRAS and NRAS (*SI Appendix*, Fig. S4*J*), which are amenable to mutant KRAS-induced negative feedback inhibition and have been recently shown to exhibit increased activation following $KRAS^{G12C}$ inhibition (66, 67). Indeed, we found that BI-3406, a selective SOS1 inhibitor, enhanced the AMG 510-induced growth suppression in MIA PaCa-2 cells (Fig. 4*D* and *SI Appendix*, Fig. S5*A*). We also obtained similar results using NCI-H358, a $KRAS^{G12C}$ non–small cell lung cancer model (*SI Appendix*, Fig. S5*B*, *Left*). Expectedly, SUIT2 PDAC cells with $KRAS^{G12D}$ were completely resistant to the drug combination (*SI Appendix*, Fig. S5*B*, *Right*). SOS1 inhibition may impair GDP-to-GTP $KRAS^{G12C}$ cycling, thereby increasing the efficacy of AMG 510 through increased availability of its substrate rather than direct inhibition of WT RAS (68). To validate the effect of SOS1 inhibition on WT RAS specifically, we employed our FPC model, which precludes the contribution of mutant KRAS GTP loading through genetic deletion of $KRAS^{G12V}$. $Kras^{G12V}$ deletion combined with SOS1 inhibition abrogated the proliferation of FPC cells (Fig. 4*E* and *SI Appendix*, Fig. S5*C*), thereby supporting the notion that the blockade or loss of oncogenic KRAS eliminates negative feedback signaling on WT RAS. Notably, excision of mutant RAS modestly enhanced the effect of trametinib in these cells (*SI Appendix*, Fig. S5*D*). The efficacy of SOS1 inhibition upon the loss of endogenous mutant KRAS implicates WT RAS in mediating the adaptive response to oncogenic KRAS-directed therapies and suggests combination strategies involving dual targeting of oncogenic KRAS and WT RAS in KRAS-driven cancers. Finally, we sought to determine whether, similarly to membrane-targeted RSK, pharmacological blockade of WT RAS signaling would attenuate downstream RAS effector pathways upon ablation of oncogenic KRAS. Indeed, treatment with 5 μM BI-3406 following the excision of endogenous mutant KRAS abolished both ERK and AKT activation, consistent with the inhibition of WT RAS signaling (Fig. 4*F*). Our findings collectively provide support for a model in which oncogenic KRAS elicits negative feedback on WT RAS through NF1/RSK1 (Fig. 5*A*). The loss of this feedback signaling through oncogenic KRAS deletion or blockade disinhibits WT RAS and provides a mechanism for adaptive resistance to oncogenic KRAS-directed therapies (Fig. 5*B*).

Discussion

While prior BirA-RAS studies have included other RAS isoforms and cell types, our experiments focused on PDAC to identify relevant mutant KRAS interactors in this malignancy (46, 47). In addition, the normalization of peptide counts to the detection of BirA increased the robustness of the analyses as suggested by the detection of internal and positive controls. It is notable that some biotinylated proteins, such as p110-α, could not be verified by MS, suggesting that the sensitivity of MS may be below the threshold for certain proteins and therefore additional fractionation methods should be considered for future BioID-MS work. Nonetheless, our approach identified 32 candidate interactors of $KRAS^{G12D}$, 11 of which have been previously reported. Our work showed that ARAF differs from the other RAF family kinases, BRAF and RAF1, by being predominantly membrane-localized with mutant RAS. Since membrane-bound ARAF is transforming even in the absence of active KRAS, this prompts further investigation of potential unique functional roles of ARAF. Other notable mutant- and membrane-specific interactors include the mTORC2 complex described by Kovalski et al. and RSK1, of which we focused on the latter (47).

While RSK1 is known to be involved in the RAS pathway downstream of ERK1/2 (60), RSK1 does not have an annotated RBD. Additionally, RSK has been previously described to have negative feedback effects on the RAS pathway via both inhibition of SOS1 and activation of NF1 in the context of WT RAS (61, 65). Although RSK1 and NF1 have been previously described to work in parallel to feedback inhibit WT RAS, our findings reveal an interaction between NF1 and RSK1. We demonstrate that the RSK1 interaction with $KRAS^{G12D}$ requires the expression of NF1 and SPRED2, suggesting the existence of a protein complex composed of mutant KRAS, NF1, RSK1, and SPRED2. Experiments with the MEK inhibitor trametinib further show that the proximity of RSK1 to $KRAS^{G12D}$ depends on ERK signaling, consistent with previous studies indicating that RSK1 activity is downstream of ERK (60, 69). RSK1 has been previously shown to transiently localize to the membrane upon EGF stimulation, and its interaction with NF1 and KRAS may mechanistically explain this observation (59). We show that membrane targeting of RSK1 does not impair the proliferation of KRAS mutant PDAC cells. However, pharmacological blockade or genetic ablation of mutant KRAS sensitizes PDAC cells to growth suppression by membrane-localized RSK1, consistent with RSK1 acting as a negative regulator of WT RAS signaling.

We demonstrate that oncogenic KRAS engages NF1/RSK1 to feedback inhibit WT RAS signaling. Consequently, the pharmacological targeting of oncogenic KRAS would disengage this negative feedback pathway, activate WT RAS, and trigger adaptive resistance. Indeed, we provide evidence that PDAC cells survive the deletion of endogenous $KRAS^{G12V}$ mutant in vitro; however, concomitant blockade of WT RAS through SOS1 inhibition completely impairs the fitness of these tumor cells. Additionally, we show that blockade of WT RAS either by expressing membrane RSK1 or pharmacologically through SOS1 inhibition enhances the efficacy of AMG 510, a selective $KRAS^{G12C}$ inhibitor, in $KRAS^{G12C}$-mutant tumor cells. Our work complements recent studies that demonstrate synergy between $KRAS^{G12C}$ inhibitors and blockade of upstream activators of WT RAS, such as EGFR or SHP2, and suggests that activation of WT RAS may play a dominant role in the adaptive resistance to oncogenic KRAS-directed therapies (68, 70).

While we demonstrate that membrane-localized RSK1 attenuates WT RAS signaling, the importance of membrane-bound RSK1 during tumor progression in KRAS mutant cells remains to be determined. We show that one role for membrane-bound RSK1 is to inhibit the signaling through WT RAS proteins during mitogenesis. This may focus biochemical effectors on mutant RAS oncoproteins to drive cancer. Alternatively, membrane-localized RSK paralogs (particularly RSK1 and RSK2) have been shown to promote invasion and metastasis of cancer cells (71). Indeed, RSK1 with prolonged membrane localization may have a greater opportunity to phosphorylate membrane-localized substrates that promote cellular functions associated with tumorigenesis, including increased cell proliferation, survival, migration, and glycolytic flux (71–76). This would implicate a function for the NF1 tumor suppressor protein in RAS-mutant cells. Consistent with such a function is that biallelic mutations and complete suppression of NF1 is rare in cancer (77). In conclusion, membrane-localized RSK1 may promote cancer in several ways in vivo. This motivates further study of the role of the NF1/RSK1 pathway in mutant KRAS-driven PDAC.

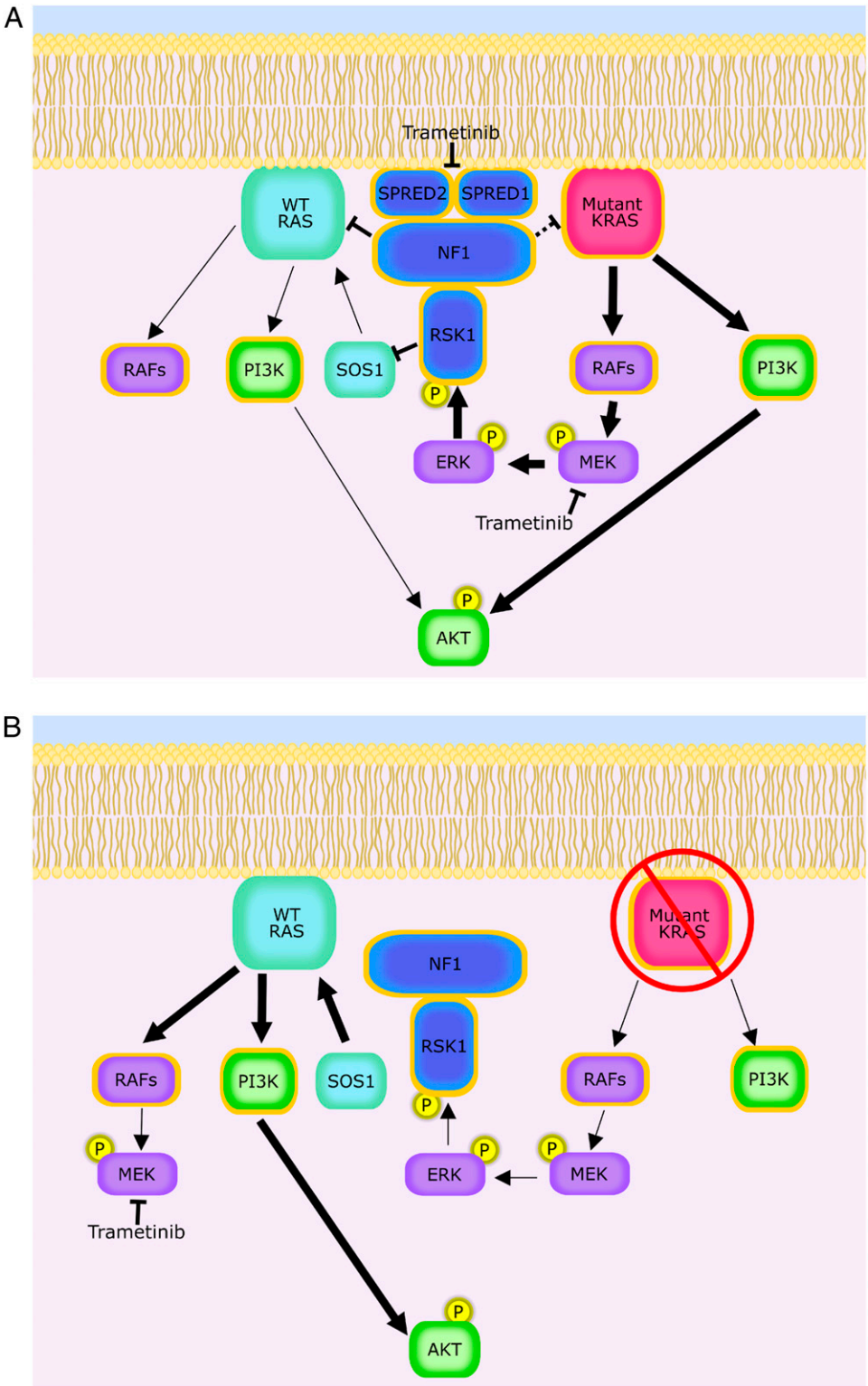

Fig. 5. Oncogenic KRAS engages an RSK1/NF1 pathway to inhibit WT RAS in pancreatic cancer cells. Schematics illustrating RSK1/NF1 interactions and known mechanisms of RSK1-mediated negative feedback on the RAS pathway. Mutant KRAS activates the RAF/MEK/ERK/RSK and PI3K/AKT pathways. Upon ERK activation, RSK1 transiently localizes to the membrane (59). (*A*) In KRAS-mutant PDAC cells, RSK1 depends on MEK activity and NF1/SPRED2 expression to be recruited to the mutant-KRAS interactome on the membrane. Membrane-localized RSK1 negatively regulates RAS activation by inhibiting the RasGEF, SOS1, and activating the RasGAP, NF1. Compared to mutant RAS, WT RAS exhibits greater sensitivity to RasGEFs and RasGAPs; therefore, the RSK1-mediated negative feedback mechanism potently inhibits WT RAS but not mutant RAS. (*B*) Upon mutant *Kras* ablation, decreased SPRED2 expression and ERK-mediated RSK1 phosphoactivation disengages the negative feedback exerted on WT RAS by NF1/RSK1, thereby enabling RAS-addicted cells to survive.

Materials and Methods

Constructs. The BirA R118G biotin-protein ligase gene including the multiple cloning site was cloned from the pcDNA3.1 mycBioID plasmid deposited by the Roux laboratory. Murine *Kras* was inserted between the multiple cloning site of BirA R118G and SalI with GGCGGAAGCGGA, encoding for a short glycine linker (GGSG). The C185S mutation was made with the Q5 Site-Directed Mutagenesis Kit. BirA-CAAX control was created by fusing the last 20 amino acids of murine KRAS4B to the C terminus of BirA. The constructs were moved to pBABE-neo between BamHI and SalI for retroviral production. For RSK1 overexpression, human RSK1 complementary DNA (cDNA) was obtained from John Blenis via Addgene. The sequence (gggagt agcaagagcaagcctaaggaccccagccagcgc) was added after the start codon of the RSK1 cDNA to fuse a myr-tag to the N terminus. Both RSK1 and myr-RSK1 were cloned into pBABE-neo between EcoRI and SalI. For gene editing, lentiCas9-Blast (addgene no. 52962, deposited by the Feng Zhang laboratory) was used (78). Guides were designed using the Benchling CRISPR tool against the first coding exon of each target gene with the best off-target

scores inserted into the ipUSEPR lentiviral vector (*SI Appendix*, Table S4). Kinase-dead RSK plasmid was constructed by PCR-based cloning. Using p-BABE-RSK plasmid as a template, the primer containing the mutations (CATCTTGGTCCGGACGCGGTCACGTACTTTCAGCGTTGCCTTCTTCAGCACGCG-CATAGCATACAGGTGCCCAC) and 5′ pBABE-RSK1 primer were used to amplify the PCR products. The PCR products digested with EcoRI/BPEBI and MfeI/BSM were subsequently subcloned into p-BABE-hRSK vector digested with EcoRI/BPEBI and MfeI/BSMI, respectively. The mutations were confirmed by Sanger sequencing.

Cell Culture. Phoenix, 293T, 3T3, mT42, mT93, mT95, and SUIT2 cells were cultured in Dulbecco's Modified Eagle Medium (DMEM) with 10% fetal bovine serum (FBS) at 37 °C in 5% CO_2 incubator. MIA PaCa-2 cells were cultured in Roswell Park Memorial Institute Medium (RPMI 1640) with 10% FBS. Cells for BioID experiments had their media changed to serum-free DMEM with 50 μM biotin for 24 h prior to cell harvest.

Cell Lysis for Protein. Cells were washed five times with ice-cold phosphate-buffered saline (PBS) prior to lysis with mild buffer (50 mM 4-(2-hydroxyethyl)-1-piperazineethanesulfonic acid (HEPES), 150 mM NaCl, 0.7% Nonidet P-40, 10% Glycerol, 1mM ethylenediaminetetraacetic acid (EDTA) with Roche cOmplete Mini protease inhibitor tablet and Roche PhoSTOP phosphatase inhibitor. Lysates were spun at 16,900 × *g* for 10 min. The detergent-compatible (DC) Protein Assay (Bio-Rad) was used to quantify the protein concentration. For experiments using FPC cells, 2 μM of 4-hydroxytamoxifen (4-OHT) with DMSO as the vehicle was added to the media for 3 d prior to harvest. AMG 510 (Selleckchem, no. S8830) dissolved in DMSO was added to RPMI for 24 h or as indicated in MIA PaCa-2 experiments. Buffers and protocol for sequential cell fractionation experiments were followed as laid out in Baghirova et al. (53)

Pulldown and Immunoprecipitation. Cell lysates were harvested in mild Nonidet P-40 buffer with protease and phosphatase inhibitor as described above (50mM HEPES, 150 mM NaCl, 0.7% Nonidet P-40, 10% Glycerol, 1mM EDTA) with Roche cOmplete Mini protease inhibitor tablet and Roche PhoSTOP phosphatase inhibitor, at 0 °C. A total of 5 mg lysate in 1 mL total buffer was incubated with 30 μl MyOne Streptavidin C1 Dynabeads or 5 mg Myc-Tag (9B11) Mouse mAb (Cell Signaling, no. 2276) antibody for 3 h with subsequent 1-h incubation with 30 μl Protein G Dynabeads for streptavidin pulldown and myc-tag immunoprecipitation (IP), respectively. The beads were washed five times in lysis buffer before elution in NuPAGE 3-(N-morpholino)propanesulfonic acid (MOPS) sodium dodecyl sulfate (SDS) running buffer at 95 °C.

MS Analysis. On-bead tryptic digestion of Dynabeads, liquid chromatography with tandem mass spectrometry (LC-MS/MS), and database searching is detailed in *SI Appendix*. Proteins quantified by only one peptide were omitted from further analysis. All quantification of peptides was normalized to that of BirA prior to producing relative enrichment by ratiometric analysis. The proteins were ranked by relative enrichment for each biological replicate. The sum of the three assigned ranks was used to indicate a general enrichment score for all three biological replicates to account for protein expression differences across cell lines. The candidate interactors were then sorted by their cumulative rank scores to identify consistently enriched interactors. Candidate interactors met their respective criteria if they were enriched in two of three biological replicates.

Cell Proliferation Assay. Mouse cell lines (3T3 cells and FPC cells) were plated at 1,000 cells per well while human cell lines (MIA PaCa-2, SUIT-2, and NCI-H358) were plated at 2,000 cells per well. Five wells were used for technical replicates. Pharmacological agents were added by HP D300 drug dispenser, and cell viability was assayed daily using the CellTiter-Glo Assay and read on a Spectramax i3 plate reader. For crystal violet staining, cells were plated in 6-well plates at a density of 5,000 cells per well and allowed to grow for 2 d or 2,000 cells per well for 3 d. The cells were washed with ice-cold PBS twice before methanol fixation for 20 min. These cells were then stained with a crystal violet solution (0.5% crystal violet, 95% ethanol in water).

Statistical Analysis. Microsoft Excel and GraphPad Prism were used for graphical representation of data. Statistical analysis was performed using Student's *t* test.

Data Availability. All study data are included in the article and/or *SI Appendix*.

ACKNOWLEDGMENTS. We thank Dr. John Blenis, Dr. Joe W. Ramos, and Dr. Channing Der for advice. We acknowledge the Cold Spring Harbor Laboratory Microscopy and Mass Spectrometry Shared Resources, which are supported by the NIH Cancer Center Support Grant P30CA045508. We thank Dr. Maria De La Paz Zafra Martin from the Lucas E. Dow Lab at Weill Cornell Medicine as well as Dr. Francisco Sanchez-Rivera from the Scott Lowe Lab at Memorial Sloan Kettering Cancer Center (MSKCC) for providing cell lines. We thank members of the Tuveson Laboratory for their assistance and advice. We thank Dr. Lindsey Baker and Dr. Jonathan Kastan for proofreading the manuscript and Dr. Qing Gao for advice. D.A.T. is a distinguished scholar of the Lustgarten Foundation and Director of the Lustgarten Foundation–designated Laboratory of Pancreatic Cancer Research. D.A.T. is also supported by the Cold Spring Harbor Laboratory Association, the V Foundation, the Thompson Foundation, and the NIH (NIH P30CA45508, U01CA224013, U01CA210240, and R01CA188134). D.A.T. is supported by the Simons Foundation (552716). Y.P. is supported by the National Cancer Institute (NCI) R50CA211506. B.A. is supported by NCI F30CA200240. D.C. is supported by NCI F30CA213883. J.S.T. is supported by NCI F31CA247416. This work was also supported by the Cold Spring Harbor Laboratory and Northwell Health Affiliation (Project Lazarus).

1. Surveillance, Epidemiology, and End Results (SEER) Program (https://seer.cancer.gov/) SEER*Stat Database: Incidence - SEER Research Data, 9 Registries, Nov 2020 Sub (1975–2018) - Linked To County Attributes - Time Dependent (1990–2018) Income/Rurality, 1969–2019 Counties, National Cancer Institute, DCCPS, Surveillance Research Program, released April 2021, based on the November 2020 submission.
2. International Agency for Research on Cancer, WHO classification of tumours of the digestive system: International Agency for Research on Cancer, 2019. *5th ed. In: Tumours of the pancreas. World Health Organization*, 295–370 (2019).
3. H. Manzano *et al*., Clinical benefit with gemcitabine (GEM) as first-line therapy for patients with advanced pancreatic cancer (APC). *Ann. Oncol.* **9**, 54 (1998).
4. R. S. King, Gemcitabine. New first-line therapy for pancreatic cancer. *Cancer Pract.* **4**, 353–354 (1996).
5. R. Spadi *et al*., Current therapeutic strategies for advanced pancreatic cancer: A review for clinicians. *World J. Clin. Oncol.* **7**, 27–43 (2016).
6. Y. Loriot, P. Mordant, E. Deutsch, K. A. Olaussen, J. C. Soria, Are RAS mutations predictive markers of resistance to standard chemotherapy? *Nat. Rev. Clin. Oncol.* **6**, 528–534 (2009).
7. S. R. Hingorani *et al*., Preinvasive and invasive ductal pancreatic cancer and its early detection in the mouse. *Cancer Cell* **4**, 437–450 (2003).
8. S. R. Hingorani *et al*., Trp53R172H and KrasG12D cooperate to promote chromosomal instability and widely metastatic pancreatic ductal adenocarcinoma in mice. *Cancer Cell* **7**, 469–483 (2005).
9. N. Bardeesy *et al*., Both p16(Ink4a) and the p19(Arf)-p53 pathway constrain progression of pancreatic adenocarcinoma in the mouse. *Proc. Natl. Acad. Sci. U.S.A.* **103**, 5947–5952 (2006).
10. J. P. Morton *et al*., LKB1 haploinsufficiency cooperates with Kras to promote pancreatic cancer through suppression of p21-dependent growth arrest. *Gastroenterology* **139**, 586–597 (2010).
11. H. Ying *et al*., PTEN is a major tumor suppressor in pancreatic ductal adenocarcinoma and regulates an NF-κB-cytokine network. *Cancer Discov.* **1**, 158–169 (2011).
12. M. A. Collins *et al*., Oncogenic Kras is required for both the initiation and maintenance of pancreatic cancer in mice. *J. Clin. Invest.* **122**, 639–653 (2012).
13. M. A. Collins *et al*., Metastatic pancreatic cancer is dependent on oncogenic Kras in mice. *PLoS One* **7**, e49707 (2012).
14. H. Ying *et al*., Oncogenic Kras maintains pancreatic tumors through regulation of anabolic glucose metabolism. *Cell* **149**, 656–670 (2012).
15. J. D. Mancias, K. L. Bryant, A. C. Kimmelman, C. J. Der, KRAS: Feeding pancreatic cancer proliferation. *Trends Biochem. Sci.* **39**, 91–100 (2014).
16. B. Bournet, C. Buscail, F. Muscari, P. Cordelier, L. Buscail, Targeting KRAS for diagnosis, prognosis, and treatment of pancreatic cancer: Hopes and realities. *Eur. J. Cancer* **54**, 75–83 (2016).
17. C. J. Marshall, Ras effectors. *Curr. Opin. Cell Biol.* **8**, 197–204 (1996).
18. A. E. Karnoub, R. A. Weinberg, Ras oncogenes: Split personalities. *Nat. Rev. Mol. Cell Biol.* **9**, 517–531 (2008).
19. A. D. Cox, C. J. Der, Ras history: The saga continues. *Small GTPases* **1**, 2–27 (2010).
20. D. K. Simanshu, D. V. Nissley, F. McCormick, RAS proteins and their regulators in human disease. *Cell* **170**, 17–33 (2017).
21. I. A. Prior, P. D. Lewis, C. Mattos, A comprehensive survey of Ras mutations in cancer. *Cancer Res.* **72**, 2457–2467 (2012).
22. K. Scheffzek *et al*., The Ras-RasGAP complex: Structural basis for GTPase activation and its loss in oncogenic Ras mutants. *Science* **277**, 333–338 (1997).
23. J. S. Iwig, J. Kuriyan, Fixing a hole where the Ras gets in. *Cell* **153**, 1191–1193 (2013).
24. A. Chandra *et al*., The GDI-like solubilizing factor PDE delta sustains the spatial organization and signalling of Ras family proteins. *Nat. Cell Biol.* **14**, 148–158 (2011).Correction in: *Nat. Cell Biol.* **14**, 329 (2012).

25. M. R. Philips, Ras hitchhikes on PDE6δ. *Nat. Cell Biol.* **14**, 128–129 (2012).
26. E. Choy *et al*., Endomembrane trafficking of ras: The CAAX motif targets proteins to the ER and golgi. *Cell* **98**, 69–80 (1999).
27. S. Pells *et al*., Developmentally-regulated expression of murine K-ras isoforms. *Oncogene* **15**, 1781–1786 (1997).
28. S. J. Plowman *et al*., K-ras 4A and 4B are co-expressed widely in human tissues, and their ratio is altered in sporadic colorectal cancer. *J. Exp. Clin. Cancer Res.* **25**, 259–267 (2006).
29. J. Yan, S. Roy, A. Apolloni, A. Lane, J. F. Hancock, Ras isoforms vary in their ability to activate Raf-1 and phosphoinositide 3-kinase. *J. Biol. Chem.* **273**, 24052–24056 (1998).
30. M. P. Quinlan, S. E. Quatela, M. R. Philips, J. Settleman, Activated Kras, but not Hras or Nras, may initiate tumors of endodermal origin via stem cell expansion. *Mol. Cell. Biol.* **28**, 2659–2674 (2008).
31. E. M. Terrell *et al*., Distinct binding preferences between ras and raf family members and the impact on oncogenic ras signaling. *Mol. Cell* **76**, 872–884.e5 (2019).
32. M. Choi, H. Bien, A. Mofunanya, S. Powers, Challenges in Ras therapeutics in pancreatic cancer. *Semin. Cancer Biol.* **54**, 101–108 (2019).
33. J. M. Ostrem, U. Peters, M. L. Sos, J. A. Wells, K. M. Shokat, K-Ras(G12C) inhibitors allosterically control GTP affinity and effector interactions. *Nature* **503**, 548–551 (2013).
34. V. Chung *et al*., Effect of selumetinib and MK-2206 vs oxaliplatin and Fluorouracil in patients with metastatic pancreatic cancer after prior therapy: SWOG S1115 study randomized clinical trial. *JAMA Oncol.* **3**, 516–522 (2017).
35. C. D. Britten, PI3K and MEK inhibitor combinations: Examining the evidence in selected tumor types. *Cancer Chemother. Pharmacol.* **71**, 1395–1409 (2013).
36. H. H. Jeng, L. J. Taylor, D. Bar-Sagi, Sos-mediated cross-activation of wild-type Ras by oncogenic Ras is essential for tumorigenesis. *Nat. Commun.* **3**, 1168 (2012).
37. M. R. Burgess *et al*., KRAS allelic imbalance enhances fitness and modulates MAP kinase dependence in cancer. *Cell* **168**, 817–829.e15 (2017).
38. G. Kong *et al*., Loss of wild-type Kras promotes activation of all Ras isoforms in oncogenic Kras-induced leukemogenesis. *Leukemia* **30**, 1542–1551 (2016).
39. A. Staffas, C. Karlsson, M. Persson, L. Palmqvist, M. O. Bergo, Wild-type KRAS inhibits oncogenic KRAS-induced T-ALL in mice. *Leukemia* **29**, 1032–1040 (2015).
40. E. Choi-Rhee, H. Schulman, J. E. Cronan, Promiscuous protein biotinylation by Escherichia coli biotin protein ligase. *Protein Sci.* **13**, 3043–3050 (2004).
41. K. J. Roux, D. I. Kim, M. Raida, B. Burke, A promiscuous biotin ligase fusion protein identifies proximal and interacting proteins in mammalian cells. *J. Cell Biol.* **196**, 801–810 (2012).
42. K. J. Roux, Marked by association: Techniques for proximity-dependent labeling of proteins in eukaryotic cells. *Cell. Mol. Life Sci.* **70**, 3657–3664 (2013).
43. A. J. Tietgens *et al*., Biotin ligase tagging identifies proteins proximal to E-cadherin, including lipoma preferred partner, a regulator of epithelial cell–cell and cell–substrate adhesion. *J. Cell Sci.* **127**, 885–895 (2014).
44. D. Dingar *et al*., BioID identifies novel c-MYC interacting partners in cultured cells and xenograft tumors. *J. Proteomics* **118**, 95–111 (2015).
45. V. Le Sage, A. Cinti, F. Valiente-Echeverría, A. J. Mouland, Proteomic analysis of HIV-1 Gag interacting partners using proximity-dependent biotinylation. *Virol. J.* **12**, 138 (2015).
46. H. Adhikari, C. M. Counter, Interrogating the protein interactomes of RAS isoforms identifies PIP5K1A as a KRAS-specific vulnerability. *Nat. Commun.* **9**, 3646 (2018).
47. J. R. Kovalski *et al*., The functional proximal proteome of oncogenic ras includes mTORC2. *Mol. Cell* **73**, 830–844.e12 (2019).
48. C. Ritchie *et al*., Analysis of K-ras interactions by biotin ligase tagging. *Cancer Genomics Proteomics* **14**, 225–239 (2017).
49. J. F. Hancock, K. Cadwallader, H. Paterson, C. J. Marshall, A CAAX or a CAAL motif and a second signal are sufficient for plasma membrane targeting of ras proteins. *EMBO J.* **10**, 4033–4039 (1991).
50. M. Liu *et al*., Targeting the protein prenyltransferases efficiently reduces tumor development in mice with K-RAS-induced lung cancer. *Proc. Natl. Acad. Sci. U.S.A.* **107**, 6471–6476 (2010).
51. C. A. Rowell, J. J. Kowalczyk, M. D. Lewis, A. M. Garcia, Direct demonstration of geranylgeranylation and farnesylation of Ki-Ras in vivo. *J. Biol. Chem.* **272**, 14093–14097 (1997).
52. T. J. Humpton *et al*., Oncogenic KRAS induces NIX-mediated mitophagy to promote pancreatic cancer. *Cancer Discov.* **9**, 1268–1287 (2019).
53. S. Baghirova, B. G. Hughes, M. J. Hendzel, R. Schulz, Sequential fractionation and isolation of subcellular proteins from tissue or cultured cells. *MethodsX* **2**, 440–445 (2015).
54. E. C. Lerner *et al*., Ras CAAX peptidomimetic FTI-277 selectively blocks oncogenic Ras signaling by inducing cytoplasmic accumulation of inactive Ras-Raf complexes. *J. Biol. Chem.* **270**, 26802–26806 (1995).
55. C. D. Go *et al*., A proximity biotinylation map of a human cell. *bioRxiv* [Preprint] (2019). 10.1101/796391 (Accessed 1 August 2020).
56. I. B. Stowe *et al*., A shared molecular mechanism underlies the human rasopathies Legius syndrome and Neurofibromatosis-1. *Genes Dev.* **26**, 1421–1426 (2012).
57. A. I. McClatchey, K. Cichowski, SPRED proteins provide a NF-ty link to Ras suppression. *Genes Dev.* **26**, 1515–1519 (2012).
58. C. Hauge, M. Frödin, RSK and MSK in MAP kinase signalling. *J. Cell Sci.* **119**, 3021–3023 (2006).
59. S. A. Richards, V. C. Dreisbach, L. O. Murphy, J. Blenis, Characterization of regulatory events associated with membrane targeting of p90 ribosomal S6 kinase 1. *Mol. Cell. Biol.* **21**, 7470–7480 (2001).
60. A. Shimamura, B. A. Ballif, S. A. Richards, J. Blenis, Rsk1 mediates a MEK-MAP kinase cell survival signal. *Curr. Biol.* **10**, 127–135 (2000).
61. M. Saha *et al*., RSK phosphorylates SOS1 creating 14-3-3-docking sites and negatively regulating MAPK activation. *Biochem. J.* **447**, 159–166 (2012).
62. T. A. Farazi, G. Waksman, J. I. Gordon, The biology and enzymology of protein N-myristoylation. *J. Biol. Chem.* **276**, 39501–39504 (2001).
63. S. J. Leevers, H. F. Paterson, C. J. Marshall, Requirement for Ras in Raf activation is overcome by targeting Raf to the plasma membrane. *Nature* **369**, 411–414 (1994).
64. J. Canon *et al*., The clinical KRAS(G12C) inhibitor AMG 510 drives anti-tumour immunity. *Nature* **575**, 217–223 (2019).
65. A. Hennig *et al*., Feedback activation of neurofibromin terminates growth factor-induced Ras activation. *Cell Commun. Signal.* **14**, 5 (2016).
66. M. B. Ryan *et al*., Vertical pathway inhibition overcomes adaptive feedback resistance to $KRAS^{G12C}$ inhibition. *Clin. Cancer Res.* **26**, 1633–1643 (2020).
67. F. E. M. Froeling *et al*., Bioactivation of napabucasin triggers reactive oxygen species-mediated cancer cell death. *Clin. Cancer Res.* **25**, 7162–7174 (2019).
68. C. Fedele *et al*., SHP2 inhibition diminishes KRASG12C cycling and promotes tumor microenvironment remodeling. *J. Exp. Med.* **218**, e20201414 (2021).
69. P. P. Roux, S. A. Richards, J. Blenis, Phosphorylation of p90 ribosomal S6 kinase (RSK) regulates extracellular signal-regulated kinase docking and RSK activity. *Mol. Cell. Biol.* **23**, 4796–4804 (2003).
70. V. Amodio *et al*., EGFR blockade reverts resistance to $KRAS^{G12C}$ inhibition in colorectal cancer. *Cancer Discov.* **10**, 1129–1139 (2020).
71. F. J. Sulzmaier, J. W. Ramos, RSK isoforms in cancer cell invasion and metastasis. *Cancer Res.* **73**, 6099–6105 (2013).
72. U. Doehn *et al*., RSK is a principal effector of the RAS-ERK pathway for eliciting a coordinate promotile/invasive gene program and phenotype in epithelial cells. *Mol. Cell* **35**, 511–522 (2009).
73. S. Tanimura *et al*., SH3P2 is a negative regulator of cell motility whose function is inhibited by ribosomal S6 kinase-mediated phosphorylation. *Genes Cells* **16**, 514–526 (2011).
74. T. Houles *et al*., RSK regulates PFK-2 activity to promote metabolic rewiring in melanoma. *Cancer Res.* **78**, 2191–2204 (2018).
75. T. Houles, P. P. Roux, Defining the role of the RSK isoforms in cancer. *Semin. Cancer Biol.* **48**, 53–61 (2018).
76. A. Méant *et al*., Proteomic analysis reveals a role for RSK in p120-catenin phosphorylation and melanoma cell-cell adhesion. *Mol. Cell. Proteomics* **19**, 50–64 (2020).
77. L. T. McGillicuddy *et al*., Proteasomal and genetic inactivation of the NF1 tumor suppressor in gliomagenesis. *Cancer Cell* **16**, 44–54 (2009).
78. N. E. Sanjana, O. Shalem, F. Zhang, Improved vectors and genome-wide libraries for CRISPR screening. *Nat. Methods* **11**, 783–784 (2014).